



OPEN ACCESS

EDITED BY

Keisuke Nakayama,
Kobe University, Japan

REVIEWED BY

Andrey Andreev,
V.I. Il'ichev Pacific Oceanological
Institute (RAS), Russia
Akira TAI,
Kyushu University, Japan

*CORRESPONDENCE

Dongseon Kim
dkim@kiost.ac.kr

SPECIALTY SECTION

This article was submitted to
Marine Biogeochemistry,
a section of the journal
Frontiers in Marine Science

RECEIVED 16 June 2022

ACCEPTED 25 July 2022

PUBLISHED 11 August 2022

CITATION

Kim D, Lee S-E, Cho S, Kang D-J,
Park G-H and Kang SK (2022)
Mesoscale eddy effects on sea-air CO₂
fluxes in the northern Philippine Sea.
Front. Mar. Sci. 9:970678.
doi: 10.3389/fmars.2022.970678

COPYRIGHT

© 2022 Kim, Lee, Cho, Kang, Park and
Kang. This is an open-access article
distributed under the terms of the
[Creative Commons Attribution License
\(CC BY\)](https://creativecommons.org/licenses/by/4.0/). The use, distribution or
reproduction in other forums is
permitted, provided the original
author(s) and the copyright owner(s)
are credited and that the original
publication in this journal is cited, in
accordance with accepted academic
practice. No use, distribution or
reproduction is permitted which does
not comply with these terms.

Mesoscale eddy effects on sea-air CO₂ fluxes in the northern Philippine Sea

Dongseon Kim*, Seon-Eun Lee, Sosul Cho, Dong-Jin Kang,
Geun-Ha Park and Sok Kuh Kang

Marine Environment and Climate Research Division, Korea Institute of Ocean Science &
Technology, Busan, South Korea

To determine the effects of mesoscale eddies on sea-air CO₂ flux, we investigated the surface fugacity of CO₂ (surface *f*CO₂) distribution in the northern Philippine Sea, where mesoscale eddies are common. Surface *f*CO₂ showed large spatial variations, such that values were high in the non-eddy and cyclonic eddy regions, while they were low within the anticyclonic eddy. The maximum *f*CO₂ was observed in the non-eddy region; higher *f*CO₂ values were observed in the area surrounding the cyclonic eddy than at the center of the cyclonic eddy. Within the cyclonic eddy, the contribution of dissolved inorganic carbon (DIC) enrichment because of upwelling was considerably offset by cooling. In the non-eddy region, the contribution of DIC enrichment from upwelling was rarely offset by cooling; thus, the maximum *f*CO₂ was observed in the non-eddy region. Surface *f*CO₂ showed a robust correlation with sea surface temperature (SST) within the cyclonic and anticyclonic eddies, but it did not display any correlation in the non-eddy region. Temperature was a major factor that controlled surface *f*CO₂ in the anticyclonic eddy, but this effect was absent in the cyclonic eddy. Temperature-normalized *f*CO₂ exhibited a clear negative relationship with SST in the cyclonic eddy and the non-eddy region, indicating that surface *f*CO₂ was considerably affected by the upwelling of high-*f*CO₂ deep water in both regions. Sea-air CO₂ fluxes ranged from 0.011 to 9.92 mmol m⁻² day⁻¹ and all values were positive, indicating that the entire study area acted as a CO₂ source during the research period. The estimated mean sea-air CO₂ fluxes in the cyclonic eddy, anticyclonic eddy, and non-eddy region were 1.10 ± 0.75, 0.64 ± 0.66, and 1.42 ± 1.12 mmol m⁻² day⁻¹, respectively. The sea-air CO₂ fluxes considerably varied according to eddy type; they were almost twofold higher in the cyclonic eddy than in the anticyclonic eddy. In the cyclonic eddy and non-eddy regions, upwelling caused surface *f*CO₂ to increase, thereby increasing sea-air CO₂ flux.

KEYWORDS

cyclonic eddy, anticyclonic eddy, sea-air CO₂ flux, surface *f*CO₂, philippine sea

Introduction

The Philippine Sea is a marginal sea bounded by the Philippines and Taiwan to the west, the Ryukyu Island arc to the north, and the Izu–Mariana Ridge to the east (Ramp et al., 2017). This sea is oceanographically bounded by the North Equatorial Current to the south, Kuroshio Current to the west, and Ryukyu Current to the north (Yaremchuk and Qu, 2004; Andres et al., 2008; Ramp et al., 2017). The Subtropical Counter Current (STCC) flows eastward in the Philippine Sea; it is present at shallow depths (~100 m) around 17–27°N latitude and 130–180°E longitude (Chang and Oey, 2014). The STCC region contains cyclonic and anticyclonic eddies with diameters of ~300 km that propagate westward at approximately 8–10 km day⁻¹ (Chelton et al., 2011). These STCC eddies have large impacts on ocean circulation in the western North Pacific Ocean (Zhang et al., 2001; Miyazawa et al., 2008; Sheu et al., 2010).

In the open ocean, mesoscale eddies have considerable impacts on surface fugacity of CO₂ ($f\text{CO}_2$) and sea-air CO₂ flux (Mahadevan et al., 2004; Gonzalez-Davila et al., 2006; Chen et al., 2007; Song et al., 2016; Moreau et al., 2017; Orselli et al., 2019). In cyclonic eddies, the uplift of subsurface waters may initially increase surface $f\text{CO}_2$, but this increase is largely offset by the lower temperature and biological productivity of the uplifted waters (Mahadevan et al., 2004); they have suggested that the vertical transport of dissolved inorganic carbon (DIC), temperature, and nitrate, as well as their contributions to surface $f\text{CO}_2$, mainly depend on their vertical gradients below the mixed layer. In the subtropical North Pacific Ocean, a negative relationship between sea surface temperature (SST) and surface $f\text{CO}_2$ is observed in a cold cyclonic eddy; the magnitude of the CO₂ sink decreases by 17% with the passage of a mesoscale cyclonic eddy (Chen et al., 2007). In the subtropical North Atlantic Ocean, surface $f\text{CO}_2$ is 15 μatm lower inside the cyclonic eddy than in surrounding waters (Gonzalez-Davila et al., 2006). In the South Atlantic Ocean, anticyclonic eddies serve as CO₂ sinks relative to the surrounding waters (Orselli et al., 2019). In the Southern Ocean, eddy effects on sea-air CO₂ fluxes are rather complex; compared with cyclonic eddies, anticyclonic eddies take up more CO₂ during summer (this relationship is reversed in winter), and anticyclonic eddies exhibit more outgassing than do cyclonic eddies (Song et al., 2016). In the open ocean, therefore, the impacts of mesoscale eddies on sea-air CO₂ fluxes are not simple; the overall sign and magnitude depend on a complex balance of physical and biological processes.

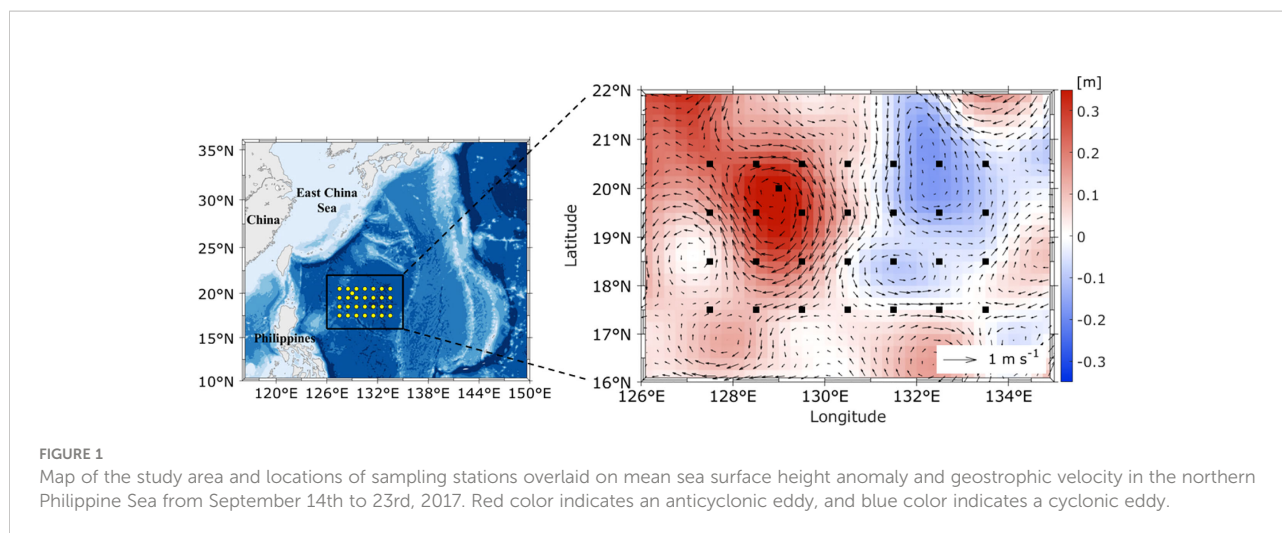
Several researchers have reported that surface $f\text{CO}_2$ is nearly equilibrated with atmospheric CO₂ in the Philippine Sea; therefore, the sea-air CO₂ flux is near zero (Inoue et al., 1995; Ishii et al., 2001; Takahashi et al., 2009; Ishii et al., 2014; Yasunaka et al., 2019). No zonal survey of surface $f\text{CO}_2$ has been conducted in the STCC region of the Philippine Sea where

both cyclonic and anticyclonic eddies are abundant. These mesoscale eddies can affect the zonal distribution of surface $f\text{CO}_2$ and sea-air CO₂ flux in the Philippine Sea. In this study, we conducted a zonal survey of surface $f\text{CO}_2$ in the northern Philippine Sea where cyclonic and anticyclonic eddies frequently occur. We identified the major factors that control surface $f\text{CO}_2$ in the northern Philippine Sea. In addition, we explored how surface $f\text{CO}_2$ was affected by changes in SST, sea surface salinity (SSS), DIC, and total alkalinity (TA). Finally, we characterized the sea-air CO₂ flux in cyclonic eddy, anticyclonic eddy, and non-eddy regions to elucidate the effects of mesoscale eddies on sea-air CO₂ flux in the northern Philippine Sea.

Materials and methods

This study was conducted on the R/V ISABU in the northern Philippine Sea from September 14th to 23rd, 2017 (Figure 1). Underway samples were collected using the flow-through system onboard R/V ISABU. Surface $f\text{CO}_2$ was obtained from a commercial underway pCO₂ system (Model 8050, General Oceanics Inc., FL, USA) equipped on the vessel; the system consisted of a non-dispersive infrared analyzer (Li-7000, LI-COR Inc., NE, USA) connected through an 8-port switching valve to three types of gases (standard gases, ambient air, and air equilibrated with flowing seawater). The analyzer was calibrated at 14-h intervals using three standard gases with different CO₂ concentrations (202, 350, and 447 ppm in dry air) after it had been zeroed and spanned using ultra-high-purity standard N₂ gas (zero-CO₂ gas) and 447-ppm CO₂ standard gas, respectively. The system was operated on the following cycle: 3 standard gases, 10 measurements of ambient air, 40 measurements of air equilibrated with seawater, and 3 repeats of all previous measurements except the standard gases. CO₂ measurement was conducted in mole fraction in dry air ($x\text{CO}_2$) mode at 4-min intervals, then converted into $f\text{CO}_2$ through correction for non-ideality and water vapor fraction based on the method established by Pierrot et al. (2009). Because atmospheric and seawater CO₂ measurements were not conducted concurrently, the atmospheric CO₂ value associated with each seawater measurement was linearly interpolated from the two nearest atmospheric measurement sets. Underway SST and SSS data were obtained alongside CO₂ measurements using a digital thermometer (SBE-38, Sea-Bird Scientific, WA, USA) and a thermosalinograph (SBE-45, Sea-Bird Scientific), respectively, installed near the seawater intake of the vessel.

Vertical profiles of temperature and salinity were measured with a calibrated conductivity–temperature–depth/pressure recorder (SBE-911; Sea-Bird Electronics Inc., WA, USA) at 29 stations (Figure 1). Seawater samples were collected for the measurement of DIC, TA, nitrate+nitrite (hereafter referred to as nitrate), and chlorophyll-*a* using a rosette sampler with 10-L



Niskin bottles mounted on the conductivity–temperature–depth/pressure assembly. DIC concentrations were determined using the VINDTA 3D system (Marianda, Kiel, Germany) coupled to a CO₂ coulometric titrator (Model 5011: UIC, Inc., Joliet, IL, USA). TA concentrations were determined with a potentiometric titration system (AS-ALK2, Apollo SciTech LLC, DE, USA). The measurement uncertainty of DIC and TA was evaluated on a daily basis using certified reference materials provided by the Scripps Institution of Oceanography (University of California, San Diego, CA, USA). The precisions of DIC and TA were $\pm 2 \mu\text{mol kg}^{-1}$ and $\pm 3 \mu\text{mol kg}^{-1}$, respectively. Nitrate concentrations were measured using a four-channel continuous auto-analyzer (QuAatro 39, Seal Analytical Inc., Germany). Reference materials for nitrate in seawater provided by “KANSO Technos” (Lot. No. “BV”) were measured alongside standards in each batch. The analytical error for nitrate was $\pm 0.14 \mu\text{mol kg}^{-1}$. Water samples for chlorophyll-*a* analysis were filtered through GF/F filters (47 mm, Whatman). Chlorophyll-*a* concentrations were determined using extracted filtrate mixed with 90% acetone for 24 h shipboard with a fluorometer (Trilogy; Turner Designs, USA) that had been previously calibrated against pure chlorophyll-*a* (Sigma, USA).

Temperature-normalized surface $f\text{CO}_2$ values were calculated by normalizing surface $f\text{CO}_2$ based on temperature to examine the effects of SST on the distribution of surface $f\text{CO}_2$, as suggested by Takahashi et al. (1993), using the following equation:

$$\begin{aligned} &\text{Temperature – normalized surface } f\text{CO}_2 \\ &= \text{surface } f\text{CO}_2 \exp[0.0423(\text{SST}_{\text{aver}} - \text{SST}_{\text{meas}})] \end{aligned} \quad (1)$$

where 0.0423 is the thermodynamic coefficient (Takahashi et al., 1993), SST_{aver} is the average of all underway SST

measurements within the study area (30.1°C), and SST_{meas} is the observed value for each CO₂ measurement.

Sea-air CO₂ flux was calculated using the following equations:

$$\begin{aligned} &\text{Sea – air CO}_2\text{ flux} \\ &= kK_0(\text{surface } f\text{CO}_2 - \text{atmospheric } f\text{CO}_2) \end{aligned} \quad (3)$$

$$k = 0.251 U_{10}^2 (Sc/660)^{-0.5} \quad (4)$$

where k and K_0 are the gas transfer velocity and the solubility coefficient of CO₂ in seawater, respectively (Weiss, 1974). For the coefficient k , we used the constant value (0.251) from the formulation of Wanninkhof (2014). U_{10} and Sc indicate wind speed collected at 10 m altitude and the Schmidt number, respectively. Wind speed data were obtained from an automatic weather station installed on R/V ISABU during underway CO₂ measurement.

Daily mean satellite altimeter gridded sea level anomaly data with $0.25^\circ \times 0.25^\circ$ spatial resolution were used to examine the appearance and movement of eddies; they were obtained from a data product estimated through the optimal interpolation method, which merged available measurements from multiple altimeter missions. These data are available online from the Copernicus Marine Service (<https://marine.copernicus.eu>).

Results

In the study area, two eddies (cyclonic and anticyclonic) were identified on the basis of sea surface height anomaly (SSHA) during the research period (Figure 1). SSHA is negative for a cyclonic eddy, whereas it is positive for an anticyclonic eddy. The cyclonic eddy propagated westward at a rate of 8 km day^{-1} , while the anticyclonic eddy propagated

southwestward at a rate of 6 km day⁻¹ during the research period. The widths of the anticyclonic and cyclonic eddies had ranges of 400–440 km and 120–160 km, respectively, during the research period (Figure 1). The anticyclonic eddy was stronger than the cyclonic eddy. Surface waters in the cyclonic eddy were typically colder and more saline, while they were warmer and fresher in the anticyclonic eddy (Figures 2A, B). Surface $f\text{CO}_2$ ranged from 384.2 to 406.7 μatm , with a mean of 393.2 μatm ; atmospheric $f\text{CO}_2$ varied from 379.2 to 383.1 μatm , with a mean of 381.2 μatm . Lower surface $f\text{CO}_2$ was observed in the anticyclonic eddy containing fresher and warmer waters (Figure 2C). The cyclonic eddy, with saltier and colder waters, showed moderate surface $f\text{CO}_2$ (395–400 μatm). Higher surface $f\text{CO}_2$ (> 400 μatm) was found in the area surrounding the cyclonic eddy (Figure 2C). Surface DIC concentrations ranged from 1902 to 1963 $\mu\text{mol kg}^{-1}$, with higher values in the cyclonic eddy and lower values in the anticyclonic eddy (Figure 2D). Surface TA displayed a distribution pattern similar to DIC, with a concentration range of 2237–2288 $\mu\text{mol kg}^{-1}$ (Figure 2E).

The vertical distributions of temperature, salinity, seawater density, DIC, TA, nitrate, and chlorophyll-*a* were plotted along the 19.5°N transect, where both cyclonic and anticyclonic eddies were observed (Figure 3). The upper layer from the surface to 200 m was warmer and less salty in the anticyclonic eddy than in the cyclonic eddy (Figures 3A, B). The uplifted structure of the cyclonic eddy was clearly observed from the vertical distributions of temperature, salinity, and seawater density, whereas a downwelled structure was observed in the anticyclonic eddy. DIC concentrations generally showed low values (< 1940 $\mu\text{mol kg}^{-1}$) within the upper 50 m of the anticyclonic eddy; these low values were associated with low salinity in this layer (Figure 3D). The DIC concentration was approximately 40 $\mu\text{mol kg}^{-1}$ higher at 50 m of water depth in the cyclonic eddy than at the same depth in the anticyclonic eddy. DIC exhibited a distinct downwelling pattern within the 300 m water depth of the anticyclonic eddy. TA displayed a vertical distribution similar to DIC, with a downwelling pattern within the upper 300 m of water in the anticyclonic eddy (Figure 3F). Nitrate was completely depleted

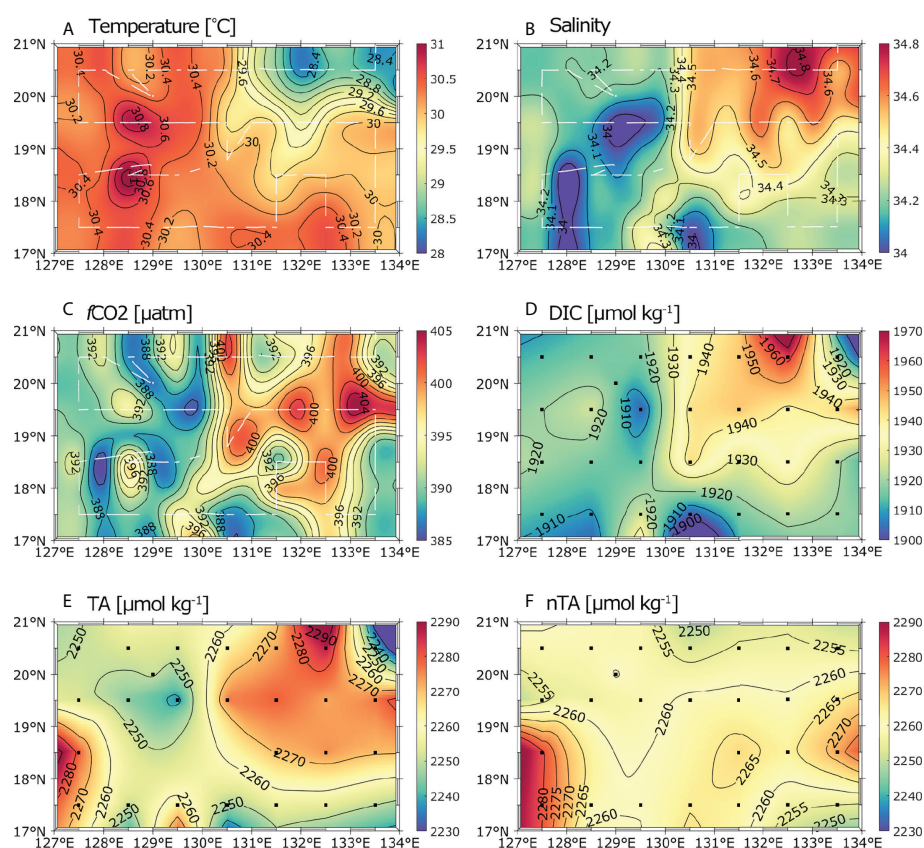


FIGURE 2

Surface distributions of temperature (A), salinity (B), $f\text{CO}_2$ (C), DIC (D), TA (E), and salinity-normalized TA (nTA, F) in the study area. Underway and discrete measurements are shown in white lines (A–C) and black dots (D, E), respectively.

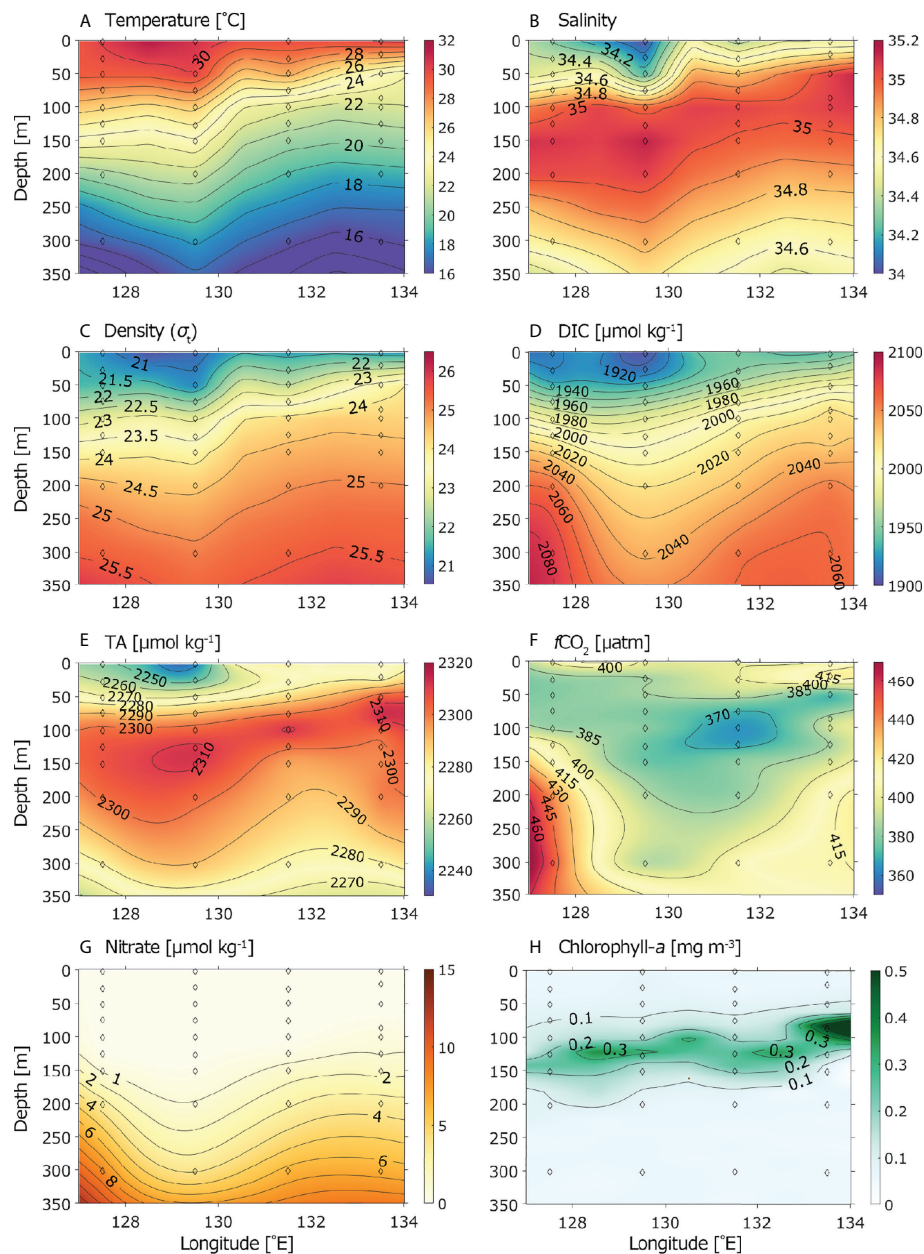


FIGURE 3

Vertical distributions of temperature (A), salinity (B), seawater density (C), DIC (D), TA (E), $f\text{CO}_2$ (F), nitrate (G), and chlorophyll-a (H) along the 19.5°N transect. Open diamonds indicate sampling depths.

within the upper 100 m of the water column in the study area, with extremely low concentrations ($< 1.0 \mu\text{mol kg}^{-1}$, Figure 3G). Nitrate showed a downwelling pattern below 150 m in depth within the anticyclonic eddy. Chlorophyll-*a* concentrations were rather low ($< 0.1 \text{ mg m}^{-3}$) and uniform within the upper 80 m of water (Figure 3H). A subsurface chlorophyll maximum was observed at the depth of 130 m in the anticyclonic eddy and at 100 m in the cyclonic eddy.

Discussion

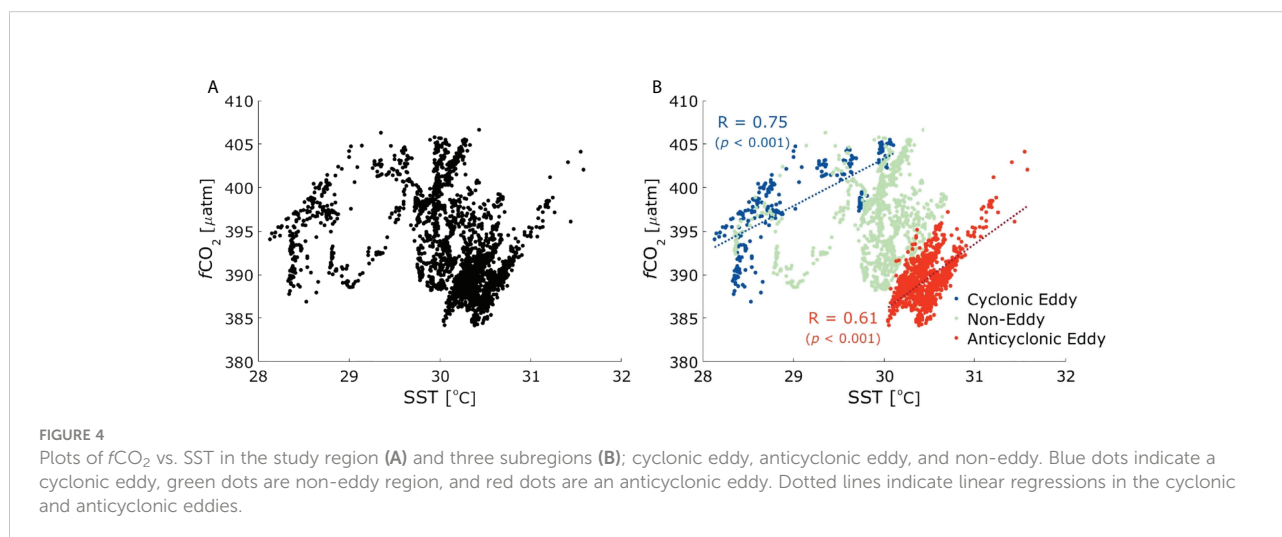
Major factors controlling the surface $f\text{CO}_2$ distribution

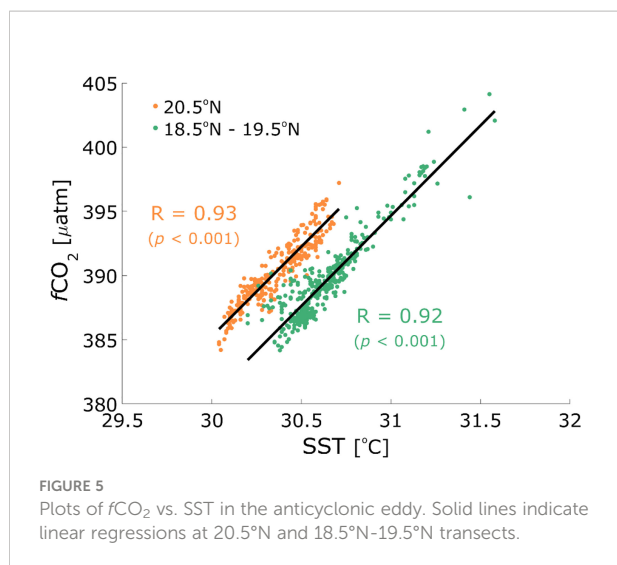
In the open ocean, surface $f\text{CO}_2$ generally exhibits a significant correlation with SST (Stephens et al., 1995; Bates et al., 1998; Nelson et al., 2001; Takahashi et al., 2002; Olsen

et al., 2004; Chen et al., 2007; Parard et al., 2016). However, in the study area, surface $f\text{CO}_2$ was not strongly correlated with SST; there was considerable variation in the data (Figure 4A). We divided the study area into three regions on the basis of SSHA: cyclonic eddy (SSHA ≤ -0.1 m), anticyclonic eddy (SSHA ≥ 0.1 m), and non-eddy (-0.1 m $<$ SSHA $<$ 0.1 m). Surface $f\text{CO}_2$ exhibited a significant correlation ($r = 0.75$, $p < 0.001$) with SST within the cyclonic eddy (Figure 4B) and a relatively strong correlation ($r = 0.61$, $p < 0.001$) within the anticyclonic eddy; it did not exhibit a correlation in the non-eddy region (Figure 4B). These results substantially differ from findings in the subtropical northeastern Pacific, where surface $f\text{CO}_2$ showed a positive linear relationship with SST outside of a cyclonic eddy and a negative relationship with SST within the cyclonic eddy (Chen et al., 2007). This discrepancy was presumably related to different vertical gradients of temperature and DIC below the mixed layer in these two areas; such gradients drive the vertical transport of temperature and DIC (Mahadevan et al., 2004).

Surface $f\text{CO}_2$ was positively linearly correlated with SST within the anticyclonic eddy, such that its values were positioned along two lines (Figure 5). These two lines were separated by approximately 5 μatm of surface $f\text{CO}_2$ at a given SST. The slopes ($\partial \ln f\text{CO}_2 / \partial T$) of those two lines were identical (0.0358), which was similar to the isochemical trend (0.0423) identified by Takahashi et al. (1993); the findings suggested that temperature was a major factor controlling surface $f\text{CO}_2$ within the anticyclonic eddy. The two lines were separated according to latitude; the upper line was located along the 20.5° N transect, while the lower line was located at the 18.5 and 19.5° N transects. SSS did not considerably differ between the two transects, but surface DIC concentrations were slightly higher along the 20.5° N transect than along the 18.5 and 19.5° N transects (Figure 2D); thus, $f\text{CO}_2$ of the upper line was 5 μatm higher at a given SST, compared with $f\text{CO}_2$ of the lower line.

Surface $f\text{CO}_2$ was also positively correlated with SST within the cyclonic eddy (Figure 4B), with a slope ($\partial \ln f\text{CO}_2 / \partial T$) of 0.0128, which was much lower than the isochemical trend (0.0423); this finding suggested that temperature was not a major factor controlling surface $f\text{CO}_2$ within the cyclonic eddy. In the plot of temperature-normalized $f\text{CO}_2$ at 30.1°C vs. SST, a negative relationship was clearly present within the cyclonic eddy (Figure 6A). This negative relationship within the cyclonic eddy may be attributed to the upwelling of high- $f\text{CO}_2$ deep water. The highest temperature-normalized $f\text{CO}_2$ value (428.4 μatm) was observed at the minimum temperature (28.2°C), which was found at the center of the cyclonic eddy. The temperature-normalized $f\text{CO}_2$ value increased by 30.4 μatm from a mean value of 398.0 μatm in the non-eddy region to the maximum value of 428.4 μatm within the cyclonic eddy because of the upwelling of cold high- $f\text{CO}_2$ deep water. When this cold high- $f\text{CO}_2$ deep water reached the surface and flowed away from the eddy center, it mixed with warm low- $f\text{CO}_2$ surface water; thus, temperature-normalized $f\text{CO}_2$ decreased with increasing SST. In addition, temperature-normalized $f\text{CO}_2$ decreased because of CO_2 efflux and biological uptake (Takahashi et al., 2002; Chen et al., 2007). The cyclonic eddy showed positive $\Delta f\text{CO}_2$ values (surface $f\text{CO}_2$ - atmospheric $f\text{CO}_2$), with a range of 5.2–24 μatm (Figure 7A); this finding indicated that CO_2 was outgassed in the study area in September 2017. Thus, the temperature-normalized $f\text{CO}_2$ might be reduced because of CO_2 efflux. Biological uptake is an important driver of decreased surface $f\text{CO}_2$ in the ocean. The upwelling of nitrate-enriched deep water may enhance biological production because nitrate is completely depleted in the surface water (Figure 3G) and DIC is consumed during biological uptake fueled by upwelled nitrate, which causes surface $f\text{CO}_2$ to decrease. In the study area, nitrate concentrations were extremely low (< 1.0 $\mu\text{mol kg}^{-1}$) within the upper 100 m of the water column and showed no uplifted structure (Figure 3G). In addition,



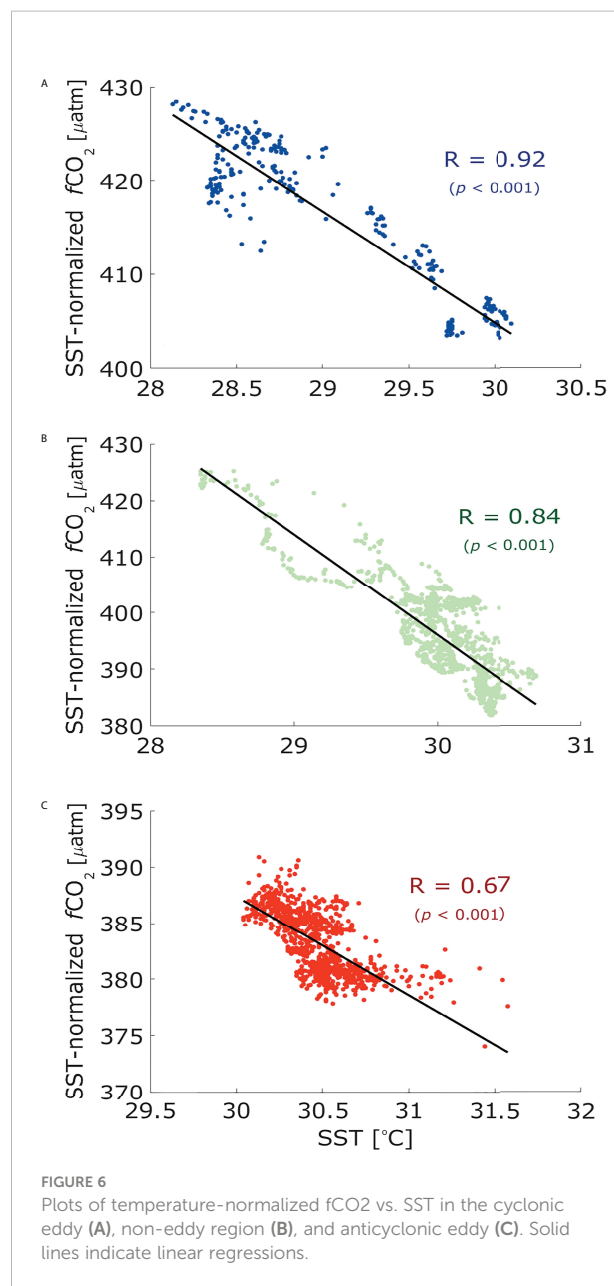


chlorophyll-*a* concentrations were rather low ($< 0.1 \text{ mg m}^{-3}$) and uniform within the upper 80 m of the water column (Figure 3H). Thus, biological uptake may not considerably influence the temperature-normalized $f\text{CO}_2$ decrease in the study area.

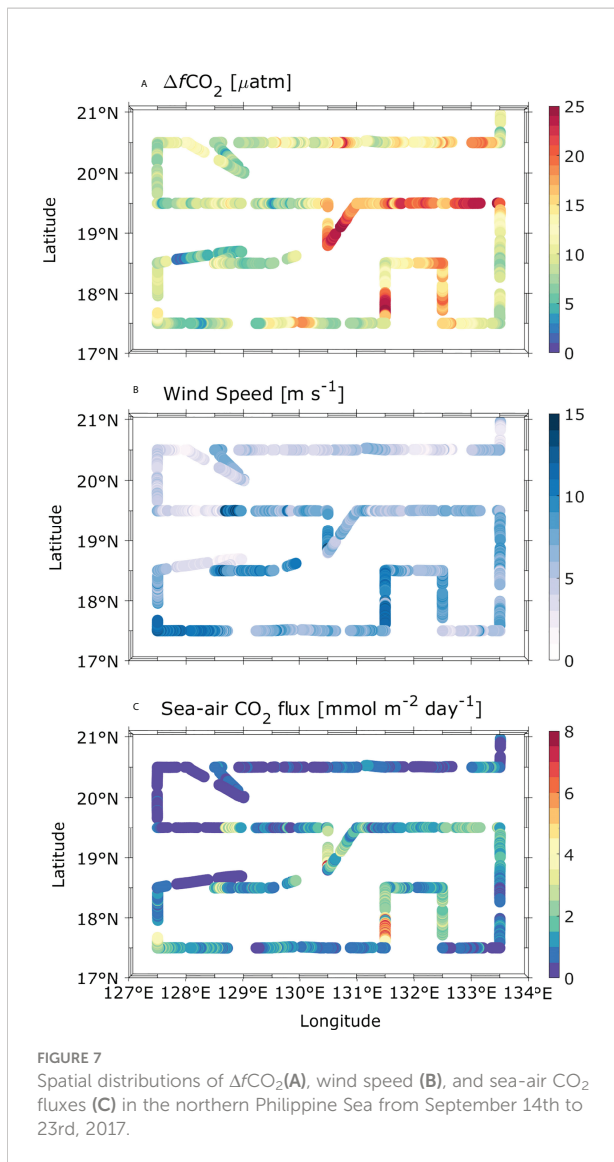
In the non-eddy region, temperature-normalized $f\text{CO}_2$ also showed a negative relationship with SST (Figure 6B). This negative relationship indicated that the non-eddy region was affected by the upwelling of high- $f\text{CO}_2$ deep water. Higher temperature-normalized $f\text{CO}_2$ values were found in the area surrounding the cyclonic eddy. Chen et al. (2007) observed that temperature-normalized $p\text{CO}_2$ values were nearly independent of the temperature outside the cyclonic eddy in the subtropical northeastern Pacific Ocean; they suggested that temperature was a major factor controlling surface $p\text{CO}_2$ in that region. Thus, surface $p\text{CO}_2$ behavior in the subtropical northeastern Pacific Ocean markedly differed from surface $p\text{CO}_2$ behavior in our study area (the northern Philippine Sea), where temperature was not a major factor controlling surface $f\text{CO}_2$ outside of the cyclonic eddy. In our study, we found that the upwelling of high- $f\text{CO}_2$ deep water considerably influenced surface $f\text{CO}_2$ in the area surrounding the cyclonic eddy. The cyclonic eddy propagated westward at a rate of 8 km day^{-1} . The area surrounding the cyclonic eddy may be affected by the upwelling of high- $f\text{CO}_2$ deep water; this possibility was corroborated by the observation of elevated temperature-normalized $f\text{CO}_2$ values only in the area surrounding the cyclonic eddy. In the the anticyclonic eddy, most temperature-normalized $f\text{CO}_2$ values were present within the narrow SST range of 30–31°C, and a weak negative relationship with SST was observed (Figure 6C).

Spatial variations of surface $f\text{CO}_2$

Surface $f\text{CO}_2$ showed high spatial variability, such that values were high in the non-eddy region and anticyclonic



eddy, while they were low within the cyclonic eddy (Figure 2C). The maximum $f\text{CO}_2$ was observed in the non-eddy region, which was located at the center of the study area (Figure 2C). Indeed, elevated surface $f\text{CO}_2$ was observed in the area surrounding the cyclonic eddy, but it was absent from the center of the cyclonic eddy (Figure 2C). The upwelled water enriched in DIC had a high $f\text{CO}_2$ value, but its impact was offset by the low temperature of the upwelled water. To determine the effect of upwelling on surface $f\text{CO}_2$ in the cyclonic eddy and non-eddy regions, we explored the effects of changes in SST, SSS, DIC, and TA on surface $f\text{CO}_2$ by using the following equation (Takahashi et al., 1993; Sarmiento and Gruber, 2006);



$$\frac{\delta p\text{CO}_2}{p\text{CO}_2} \approx \frac{1}{p\text{CO}_2} \frac{\delta p\text{CO}_2}{\delta \text{SST}} \delta \text{SST} + \frac{1}{p\text{CO}_2} \frac{\delta p\text{CO}_2}{\delta \text{SSS}} \delta \text{SSS} + \frac{1}{p\text{CO}_2} \frac{\delta p\text{CO}_2}{\delta \text{DIC}} \delta \text{DIC} + \frac{1}{p\text{CO}_2} \frac{\delta p\text{CO}_2}{\delta \text{TA}} \delta \text{TA} \approx \beta \delta \text{SST} + \alpha \frac{\delta \text{SSS}}{\text{SSS}} + \gamma_{\text{DIC}} \frac{\delta \text{DIC}}{\text{DIC}} + \gamma_{\text{TA}} \frac{\delta \text{TA}}{\text{TA}}$$

The equation used by authors (p. 7) is valid only along the water pathway (Lagrangian approach). The presented equation takes into account the changes in the seawater $p\text{CO}_2$ due to evaporation/precipitation, warming/cooling, and photosynthesis/organic matter degradation. But it does not take into account the changes in the seawater $p\text{CO}_2$ due to mixing (horizontal and vertical) with the water masses of different origin and different initial (pre-formed) values of $p\text{CO}_2$ (T, S, TA, DIC). It's necessarily to add some contents on cyclone and anticyclone water origin.

Answer: The changes in the seawater $p\text{CO}_2$ due to mixing (horizontal and vertical) with the water masses make the

changes in the DIC concentrations, and thereby, we can calculate the $p\text{CO}_2$ changes due to mixing from the DIC changes by using the Revelle factor. Thus, this equation takes into account the changes in the seawater $p\text{CO}_2$ due to mixing (horizontal and vertical) with the water masses.

where β is approximately $0.0423^\circ\text{C}^{-1}$, α is 1.0, γ_{DIC} is 9.5, and γ_{TA} is -8.9 (Sarmiento and Gruber, 2006). Assuming that upwelling was not active in the anticyclonic eddy, that eddy would be served as a reference point for the comparison of $\delta f\text{CO}_2$ values between the cyclonic eddy and non-eddy regions. Thus, the observed $\delta f\text{CO}_2$ values in the cyclonic eddy were $f\text{CO}_2$ differences between the cyclonic eddy and the anticyclonic eddy (Table 1). The observed $\delta f\text{CO}_2$ values in the non-eddy region were $f\text{CO}_2$ differences between the non-eddy region and anticyclonic eddy (Table 2). The observed $\delta f\text{CO}_2$ values closely aligned with the $\delta f\text{CO}_2$ values calculated from δSST , δSSS , δDIC , and δTA in both the cyclonic eddy and non-eddy regions (Tables 1, 2). The differences between the observed $\delta f\text{CO}_2$ and calculated $\delta f\text{CO}_2$ values were $< 10\%$ (Tables 1, 2).

Mean surface $f\text{CO}_2$ values were $12.2 \mu\text{atm}$ higher in the cyclonic eddy than in the anticyclonic eddy (Table 1). $\delta f\text{CO}_2$ increased by $65.6 \mu\text{atm}$ because of DIC enrichment driven by upwelling in the cyclonic eddy, while it decreased by $37.2 \mu\text{atm}$ because of the TA increase (Table 1). Thus, the $\delta f\text{CO}_2$ value increased by $28.4 \mu\text{atm}$ because of the combined effects of DIC and TA enrichment with upwelling in the cyclonic eddy. SST contributed a $\delta f\text{CO}_2$ decrease of $19.9 \mu\text{atm}$, while SSS contributed a $\delta f\text{CO}_2$ increase of $4.4 \mu\text{atm}$ (Table 1).

Mean surface $f\text{CO}_2$ values were $4.8 \mu\text{atm}$ higher in the non-eddy region than in the anticyclonic eddy (Table 2). $\delta f\text{CO}_2$ increased by $22.7 \mu\text{atm}$ because of the DIC increase, while it decreased by $12.4 \mu\text{atm}$ because of the TA increase (Table 2). Thus, the $\delta f\text{CO}_2$ value increased by $10.3 \mu\text{atm}$ overall because of DIC and TA increases in the non-eddy region. SST contributed a $\delta f\text{CO}_2$ decrease of $6.7 \mu\text{atm}$, while SSS contributed a $\delta f\text{CO}_2$ increase of $1.3 \mu\text{atm}$ (Table 2).

The maximum $\delta f\text{CO}_2$ value observed in the cyclonic eddy was $16.8 \mu\text{atm}$ (Table 1). The DIC and TA enrichment by upwelling contributed the $\delta f\text{CO}_2$ increase of $41.7 \mu\text{atm}$, while SST and SSS contributed the $\delta f\text{CO}_2$ decrease of $24.4 \mu\text{atm}$

TABLE 1 Observed $\delta f\text{CO}_2$, δSST , δSSS , δDIC , and δTA in the cyclonic eddy, maximum and minimum $f\text{CO}_2$ sites. Calculated $\delta f\text{CO}_2$ values from δSST , δSSS , δDIC , and δTA are shown in brackets.

	$\delta f\text{CO}_2$	δSST	δSSS	δDIC	δTA
Mean values in the cyclonic eddy	12.2 (12.8)	-1.19 (-19.9)	0.41 (4.4)	33.8 (65.6)	24.0 (-37.2)
Values at the maximum $f\text{CO}_2$ site	16.8 (17.3)	-1.84 (-30.7)	0.59 (6.3)	48.6 (94.3)	33.9 (-52.6)
Values at the minimum $f\text{CO}_2$ site	9.3 (9.7)	-0.64 (-10.7)	0.29 (3.1)	23.7 (46.0)	18.5 (-28.7)

Observed $\delta f\text{CO}_2$ values in the cyclonic eddy are $f\text{CO}_2$ differences between the cyclonic eddy and the anticyclonic eddy.

TABLE 2 Observed $\delta f\text{CO}_2$, δSST , δSSS , δDIC , and δTA in the non-eddy region, maximum and minimum $f\text{CO}_2$ sites. Calculated $\delta f\text{CO}_2$ from δSST , δSSS , δDIC , and δTA are shown in brackets.

	$\delta f\text{CO}_2$	δSST	δSSS	δDIC	δTA
Mean values in the non-eddy region	4.8 (4.9)	-0.40 (-6.7)	0.12 (1.3)	11.7 (22.7)	8.0 (-12.4)
Values at the maximum $f\text{CO}_2$ site	25.8 (26.9)	-0.25 (-4.2)	0.36 (3.9)	28.5 (55.3)	18.1 (-28.1)
Values at the minimum $f\text{CO}_2$ site	-17.1 (-19.3)	-0.47 (-7.9)	0.08 (0.9)	7.0 (13.6)	16.7 (-25.9)

Observed $\delta f\text{CO}_2$ values in the non-eddy region are $f\text{CO}_2$ differences between the non-eddy region and anticyclonic eddy.

(Table 1). In contrast, the maximum $\delta f\text{CO}_2$ value observed in the non-eddy region was 25.8 μatm (Table 2). The DIC and TA enrichment contributed the $\delta f\text{CO}_2$ increase of 27.2 μatm , while SST and SSS contributed the $\delta f\text{CO}_2$ decrease of 0.3 μatm (Table 2). In the cyclonic eddy, the contribution of DIC enrichment by upwelling was largely balanced by cooling. In the non-eddy region, however, the contribution of DIC enrichment by upwelling was rarely balanced by cooling; this was the main reason for maximum $f\text{CO}_2$ observation in the non-eddy region. DIC enrichment in the non-eddy region was presumably associated with the upwelling because it was observed in the area surrounding the cyclonic eddy.

Variations of sea-air CO_2 fluxes

$\Delta f\text{CO}_2$ (surface $f\text{CO}_2$ – atmospheric $f\text{CO}_2$) varied from 5.2 to 25.7 μatm ; it had consistently positive values. $\Delta f\text{CO}_2$ exhibited high spatial variability, such that values were high within the anticyclonic eddy and low within the cyclonic eddy (Figure 7A). Wind speed obtained from the R/V ISABU automatic weather station had a range of 0.6–15.8 m s^{-1} and exhibited high spatial variability, such that values were elevated in the non-eddy region (Figure 7B). Sea-air CO_2 fluxes were calculated from $\Delta f\text{CO}_2$ and wind speed. In the study area, sea-air CO_2 fluxes ranged from 0.011 to 9.92 $\text{mmol m}^{-2} \text{day}^{-1}$ and all values were positive, indicating that the entire study area acted as a CO_2 source during the research period (Figure 7C). The estimated mean sea-air CO_2 fluxes in the cyclonic eddy, anticyclonic eddy, and non-eddy region were 1.10 ± 0.75 , 0.64 ± 0.66 , and 1.42 ± 1.12 $\text{mmol m}^{-2} \text{day}^{-1}$, respectively. The sea-air CO_2 fluxes considerably varied according to eddy type; they were almost twofold higher in the cyclonic eddy than in the anticyclonic eddy. In the cyclonic eddy and non-eddy regions, upwelling caused surface $f\text{CO}_2$ to increase, thereby increasing sea-air CO_2 flux. However, the CO_2 flux was slightly greater in the non-eddy region than in the cyclonic eddy. The mean $\Delta f\text{CO}_2$ was higher in the cyclonic eddy than in the non-eddy region, but CO_2 flux was higher in the non-eddy region because of the high wind speed (Figure 7). In addition, maximum $\Delta f\text{CO}_2$ was observed in the

non-eddy region because the DIC enrichment caused by upwelling was rarely offset by cooling in this region.

The study area was located in the northern Philippine Sea, where surface $f\text{CO}_2$ was nearly equilibrated with atmospheric CO_2 , and the sea-air CO_2 flux was therefore rather small (< 0.6 $\text{mmol m}^{-2} \text{day}^{-1}$; Takahashi et al., 2002; Takahashi et al., 2009; Ishii et al., 2014; Yasunaka et al., 2019). In this study, CO_2 flux in the anticyclonic eddy was similar to previously reported results. However, CO_2 fluxes in the cyclonic eddy and non-eddy region were approximately twofold greater than in previous studies. The cyclonic eddy caused the CO_2 flux to increase because of the upwelling of high- $f\text{CO}_2$ deep water. In the non-eddy region, high CO_2 fluxes were observed in the area surrounding the cyclonic eddy, indicating that the non-eddy region was affected by the upwelling of high- $f\text{CO}_2$ deep water. In the study area, a cyclonic eddy with a width of 120–160 km propagated westward at a rate of 8 km day^{-1} . After the cyclonic eddy had passed, the waters surrounding the cyclonic eddy had high DIC concentrations, which caused surface $f\text{CO}_2$ to increase during the warming of cold upwelled water. Indeed, the waters surrounding the cyclonic eddy showed higher CO_2 fluxes compared with the area around the anticyclonic eddy (Figure 7C).

Conclusions

This study examined how mesoscale eddies affect surface $f\text{CO}_2$ and sea-air CO_2 flux in the northern Philippine Sea. Surface $f\text{CO}_2$ showed high spatial variability, such that values were high in the non-eddy region and cyclonic eddy, while they were low within the anticyclonic eddy. Temperature was a major factor controlling surface $f\text{CO}_2$ in the anticyclonic eddy, but such an effect was not observed in the cyclonic eddy. Surface $f\text{CO}_2$ was influenced by the upwelling of high- $f\text{CO}_2$ deep water in the non-eddy region and cyclonic eddy. In the northern Philippine Sea, surface $f\text{CO}_2$ was strongly positively correlated with SST within cyclonic and anticyclonic eddies, while it showed no correlation in the non-eddy region. In the subtropical northeastern Pacific, in contrast, surface $f\text{CO}_2$ showed a positive linear relationship with SST outside of a cyclonic eddy and a negative relationship with SST within the cyclonic eddy (Chen et al., 2007). This discrepancy was presumably related to different vertical gradients of temperature and DIC below the mixed layer in these two areas; such gradients drive the vertical transport of temperature and DIC. Therefore, the effects of mesoscale eddies on surface $f\text{CO}_2$ were highly variable in the open ocean. To overcome this problem, more intensive surveys must be conducted across broad areas of the open ocean.

In the northern Philippine Sea, a cyclonic eddy caused surface $f\text{CO}_2$ to increase because of the upwelling of high- $f\text{CO}_2$ deep water, thereby increasing local sea-air CO_2 flux, which was nearly twofold greater than the flux within an

anticyclonic eddy. However, surface $f\text{CO}_2$ and sea-air CO_2 flux were not strongly affected by the anticyclonic eddy. Numerous researchers have attempted to estimate surface $f\text{CO}_2$ and sea-air CO_2 flux in the open ocean using the general surface $f\text{CO}_2$ and SST relationship (Olsen et al., 2004; Park and Wanninkhof, 2012). However, in open-ocean areas where multiple eddies are present, sea-air CO_2 flux estimated in this manner might be considerably underestimated within cyclonic eddies and the surrounding areas because cyclonic eddies increase CO_2 flux due to the upwelling of high- $f\text{CO}_2$ deep water. Therefore, estimation of sea-air CO_2 flux using the general surface $f\text{CO}_2$ and SST relationship should be avoided in the open ocean where cyclonic eddies occur.

Data availability statement

The datasets presented in this study can be found in online repositories. The names of the repository/repositories and accession number(s) can be found below: <https://doi.org/10.22711/idr/941>.

Author contributions

DK, S-EL, and SC were responsible for data analysis and writing the manuscript. G-HP contributed with discussions and data analysis. D-JK and SSK performed a field survey and

analyzed the data set. All authors contributed to the article and approved the submitted version.

Funding

This work was supported by the project PEA0012 of the Korea Institute of Ocean Science and Technology, and in part by the project entitled ‘Study on Northwestern Pacific Warming and Genesis and Rapid Intensification of Typhoon’, funded by the Ministry of Oceans and Fisheries (20220566)

Conflict of interest

The authors declare that the research was conducted in the absence of any commercial or financial relationships that could be construed as a potential conflict of interest.

Publisher’s note

All claims expressed in this article are solely those of the authors and do not necessarily represent those of their affiliated organizations, or those of the publisher, the editors and the reviewers. Any product that may be evaluated in this article, or claim that may be made by its manufacturer, is not guaranteed or endorsed by the publisher.

References

- Andres, M., Park, J. H., Winibush, M., Zhu, X. H., Chang, K. I., and Ichikawa, H. (2008). Study of the Kuroshio/Ryukyu current system based on satellite-altimeter and *in situ* measurements. *J. Oceanogr* 64 (6), 937–950. doi: 10.1007/s10872-008-0077-2
- Bates, N. R., Takahashi, T., Chipman, D. W., and Knap, A. H. (1998). Variability of $p\text{CO}_2$ on diel to seasonal timescales in the Sargasso Sea near Bermuda. *J. Geophys Res-Ocean* 103 (C8), 15567–15585. doi: 10.1029/98jc00247
- Chang, Y. L., and Oey, L. Y. (2014). Instability of the north pacific subtropical countercurrent. *J. Phys. Oceanogr* 44 (3), 818–833. doi: 10.1175/jpo-d-13-0162.1
- Chelton, D. B., Schlax, M. G., and Samelson, R. M. (2011). Global observations of nonlinear mesoscale eddies. *Prog. Oceanogr* 91 (2), 167–216. doi: 10.1016/j.pocean.2011.01.002
- Chen, F. Z., Cai, W. J., Benitez-Nelson, C., and Wang, Y. C. (2007). Sea Surface $p\text{CO}_2$ -SST relationships across a cold-core cyclonic eddy: Implications for understanding regional variability and air-sea gas exchange. *Geophys Res. Lett.* 34 (10). doi: 10.1029/2006gl028058
- Gonzalez-Davila, M., Santana-Casiano, J. M., de Armas, D., Escanez, J., and Suarez-Tangil, M. (2006). The influence of island generated eddies on the carbon dioxide system, south of the canary islands. *Mar. Chem.* 99 (1-4), 177–190. doi: 10.1016/j.marchem.2005.11.004
- Inoue, H. Y., Matsueda, H., Ishii, M., Fushimi, K., Hirota, M., Asanuma, I., et al. (1995). Long-term trend of the partial pressure of carbon dioxide ($p\text{CO}_2$) in surface waters of the western north pacific 1984-1993. *Tell Ser. B-Chem Phys. Meteorol* 47 (4), 391–413. doi: 10.1034/j.1600-0889.47.issue4.2.x
- Ishii, M., Feely, R. A., Rodgers, K. B., Park, G. H., Wanninkhof, R., Sasano, D., et al. (2014). Air-sea CO_2 flux in the pacific ocean for the period 1990-2009. *Biogeosciences* 11 (3), 709–734. doi: 10.5194/bg-11-709-2014
- Ishii, M., Inoue, H. Y., Matsueda, H., Saito, S., Fushimi, K., Nemoto, K., et al. (2001). Seasonal variation in total inorganic carbon and its controlling processes in surface waters of the western north pacific subtropical gyre. *Mar. Chem.* 75 (1-2), 17–32. doi: 10.1016/s0304-4203(01)00023-8
- Mahadevan, A., Levy, M., and Memery, L. (2004). Mesoscale variability of sea surface $p\text{CO}_2$: What does it respond to? *Global Biogeochem Cycle* 18 (1). doi: 10.1029/2003gb002102
- Miyazawa, Y., Kagimoto, T., Guo, X. Y., and Sakuma, H. (2008). The kuroshio large meander formation in 2004 analyzed by an eddy-resolving ocean forecast system. *J. Geophys Res-Ocean* 113 (C10). doi: 10.1029/2007jc004226
- Moreau, S., Della Penna, A., Llorca, J., Patel, R., Langlais, C., Boyd, P. W., et al. (2017). Eddy-induced carbon transport across the Antarctic circumpolar current. *Global Biogeochem Cycle* 31 (9), 1368–1386. doi: 10.1002/2017gb005669
- Nelson, N. B., Bates, N. R., Siegel, D. A., and Michaels, A. F. (2001). Spatial variability of the CO_2 sink in the Sargasso Sea. *Deep-Sea Res. Part II-Top Stud. Oceanogr* 48 (8-9), 1801–1821. doi: 10.1016/s0967-0645(00)00162-4
- Olsen, A., Trinanes, J. A., and Wanninkhof, R. (2004). Sea-Air flux of CO_2 in the Caribbean Sea estimated using *in situ* and remote sensing data. *Remote Sens. Environ.* 89 (3), 309–325. doi: 10.1016/j.rse.2003.10.011
- Orsell, I. B. M., Kerr, R., de Azevedo, J. L. L., Galdino, F., Araujo, M., and Garcia, C. A. E. (2019). The sea-air CO_2 net fluxes in the south Atlantic ocean and the role played by agulhas eddies. *Prog. Oceanogr* 170, 40–52. doi: 10.1016/j.pocean.2018.10.006
- Parard, G., Charantonis, A. A., and Rutgersson, A. (2016). Using satellite data to estimate partial pressure of CO_2 in the Baltic Sea. *J. Geophys Res-Biogeosci* 121 (3), 1002–1015. doi: 10.1002/2015jg003064

- Park, G. H., and Wanninkhof, R. (2012). A large increase of the CO₂ sink in the western tropical north Atlantic from 2002 to 2009. *J. Geophys Res-Ocean* 117. doi: 10.1029/2011jc007803
- Pierrot, D., Neill, C., Sullivan, K., Castle, R., Wanninkhof, R., Luger, H., et al. (2009). Recommendations for autonomous underway pCO₂ measuring systems and data-reduction routines. *Deep-Sea Res. Part II-Top Stud. Oceanogr* 56 (8-10), 512–522. doi: 10.1016/j.dsr2.2008.12.005
- Ramp, S. R., Colosi, J. A., Worcester, P. F., Bahr, F. L., Heaney, K. D., Mercer, J. A., et al. (2017). Eddy properties in the subtropical countercurrent, Western Philippine Sea. *Deep-Sea Res. Part I-Oceanogr Res. Pap* 125, 11–25. doi: 10.1016/j.dsr.2017.03.010
- Sarmiento, J. L., and Gruber, N. (2006). *Ocean biogeochemical dynamics* (New Jersey: Princeton University Press).
- Sheu, W. J., Wu, C. R., and Oey, L. Y. (2010). Blocking and Westward passage of eddies in the Luzon Strait. *Deep-Sea Res. Part II-Top Stud. Oceanogr* 57 (19-20), 1783–1791. doi: 10.1016/j.dsr2.2010.04.004
- Song, H., Marshall, J., Munro, D. R., Dutkiewicz, S., Sweeney, C., McGillicuddy, D. J., et al. (2016). Mesoscale modulation of air-sea CO₂ flux in Drake Passage. *J. Geophys Res-Ocean* 121 (9), 6635–6649. doi: 10.1002/2016jc011714
- Stephens, M. P., Samuels, G., Olson, D. B., and Fine, R. A. (1995). Sea-Air flux of CO₂ in the north Pacific using shipboard and satellite data. *J. Geophys Res-Ocean* 100 (C7), 13571–13583. doi: 10.1029/95jc00901
- Takahashi, T., Olafsson, J., Goddard, J. G., Chipman, D. W., and Sutherland, S. C. (1993). Seasonal variation of CO₂ and nutrients in the high-latitude surface oceans: A comparative study. *Global Biogeochem Cycle* 7 (4), 843–878. doi: 10.1029/93gb02263
- Takahashi, T., Sutherland, S. C., Sweeney, C., Poisson, A., Metzler, N., Tilbrook, B., et al. (2002). Global sea-air CO₂ flux based on climatological surface ocean pCO₂, and seasonal biological and temperature effects. *Deep-Sea Res. Part II-Top Stud. Oceanogr* 49 (9-10), 1601–1622. doi: 10.1016/s0967-0645(02)00003-6
- Takahashi, T., Sutherland, S. C., Wanninkhof, R., Sweeney, C., Feely, R. A., Chipman, D. W., et al. (2009). Climatological mean and decadal change in surface ocean pCO₂, and net sea-air CO₂ flux over the global oceans. *Deep-Sea Res. Part II-Top Stud. Oceanogr* 56 (8-10), 554–577. doi: 10.1016/j.dsr2.2008.12.009
- Wanninkhof, R. (2014). Relationship between wind speed and gas exchange over the ocean revisited. *Limnol Oceanogr: Methods* 12, 351–362. doi: 10.4319/lom.2014.12.351
- Weiss, R. F. (1974). Carbon dioxide in water and seawater: the solubility of a non-ideal gas. *Mar. Chem.* 2 (3), 203–215. doi: 10.1016/0304-4203(74)90015-2
- Yaremchuk, M., and Qu, T. D. (2004). Seasonal variability of the large-scale currents near the coast of the Philippines. *J. Phys. Oceanogr* 34 (4), 844–855. doi: 10.1175/1520-0485(2004)034<0844:Svodlc>2.0.Co;2
- Yasunaka, S., Kouketsu, S., Stratton, P. G., Sutton, A. J., Murata, A., Nakaoka, S., et al. (2019). Spatio-temporal variability of surface water pCO₂ and nutrients in the tropical Pacific from 1981 to 2015. *Deep-Sea Res. Part II-Top Stud. Oceanogr* 169. doi: 10.1016/j.dsr2.2019.104680
- Zhang, D. X., Lee, T. N., Johns, W. E., Liu, C. T., and Zantopp, R. (2001). The Kuroshio east of Taiwan: Modes of variability and relationship to interior ocean mesoscale eddies. *J. Phys. Oceanogr* 31 (4), 1054–1074. doi: 10.1175/1520-0485(2001)031<1054:Tkeotm>2.0.Co;2